JACS
JOURNAL OF THE AMERICAN CHEMICAL SOCIETY
Article
pubs.acs.org/JACS

CO Oxidation Mechanism on CeO_2-Supported Au Nanoparticles

Hyun You Kim,*[,†] Hyuck Mo Lee,[‡] and Graeme Henkelman[†]

[†]Department of Chemistry and Biochemistry, University of Texas at Austin, Austin, Texas 78712-0165, United States
[‡]Department of Materials Science and Engineering, KAIST, 291 Daehak-ro, Yuseong-gu, Daejeon, Korea

Supporting Information

ABSTRACT: Density functional theory was used to study the CO oxidation catalytic activity of CeO_2-supported Au nanoparticles (NPs). Experimental observations on CeO_2 show that the surface of CeO_2 is enriched with oxygen vacancies. We compare CO oxidation by a Au_{13} NP supported on stoichiometric CeO_2 (Au_{13}@CeO_2-STO) and partially reduced CeO_2 with three vacancies (Au_{13}@CeO_2-3VAC). The structure of the Au_{13} NP was chosen to minimize structural rearrangement during CO oxidation. We suggest three CO oxidation mechanisms by Au_{13}@CeO_2: CO oxidation by coadsorbed O_2, CO oxidation by a lattice oxygen in CeO_2, and CO oxidation by O_2 bound to a Au−Ce^{3+} anchoring site. Oxygen vacancies are shown to open a new CO oxidation pathway by O_2 bound to a Au−Ce^{3+} anchoring site. Our results provide a design strategy for CO oxidation on supported Au catalysts. We suggest lowering the vacancy formation energy of the supporting oxide, and using an easily reducible oxide to increase the concentration of reduced metal ions, which act as anchoring sites for O_2 molecules.

INTRODUCTION

More than two decades have passed since Haruta's pioneering finding that supported small Au nanoparticles (NPs) catalyze CO oxidation at or below room temperature.[1] Experimental and theoretical studies on the catalytic properties of oxide-supported Au NPs have suggested thus far that the size of Au NPs,[2−5] their structural fluxionality,[6−8] their electronic interaction with supporting materials,[3,8−10] and the presence of a Au NP−support interface[7,11,12] are factors that activate supported Au NPs. Because of high computational costs and the limited resolution of experimental methods, current understanding of catalytic activity on oxide-supported Au NPs is based on highly model systems, for example, gas-phase crystalline Au NPs,[2,4] tiny Au clusters supported on oxide surfaces,[6,7,13,14] or Au NPs on clean oxide surfaces.[15]

Among the various oxides, CeO_2 has been recognized as the best supporting material for catalysis at Au NPs[15] due to its high oxygen storage and release capacity, facile oxygen vacancy formation, and the presence of a narrow Ce f-band.[15] Experimental studies have shown that the surface of CeO_2 can easily be enriched with oxygen vacancies[15−17] and that Au NPs bind strongly to these vacancies.[18] Lawrence et al. recently demonstrated that catalytic activity is a function of the concentration of oxygen vacancies for the CO oxidation activity of CeO_2 nanorods, NPs, and the bulk surface.[17] Oxygen vacancy formation on the CeO_2 surface accompanies the reduction of adjacent Ce^{4+} ions to Ce^{3+}, and the concentration of Ce^{3+} ions is proportional to that of oxygen vacancies.[17] Localized electrons on the occupied 4f-orbital of Ce^{3+} ions contribute to the electronic interaction between reduced CeO_2 and supported Au NPs.[15,19]

CeO_2-supported Au is regarded as a promising catalytic system, because it combines highly active components, Au NPs and CeO_2. To design a catalyst, a detailed analysis of catalytic activity of CeO_2-supported Au NPs is required. Several reactive species, such as lattice oxygen,[13] under-coordinated Au atoms in Au NPs,[2] and a Au ion substituting a lattice Ce ion,[20] have been independently reported as reactive species for CO oxidation by CeO_2-supported Au NPs. The local electronic state of the reactive Au species likely also plays a role.[13,21,22] The CO oxidation process by CeO_2-supported Au NPs has not, however, been systematically studied as a single system. Previous studies, which considered tiny Au clusters or Au ions, were not able to investigate the role of the atomic coordination or the morphology of Au NPs that become important as the size of the NPs increase. Even the most extensive study on the role of the under-coordinated Au atoms of Au NP was performed on Au crystallites,[2] so the effect of the CeO_2 support was missing.

Furthermore, from an industrial perspective, model systems of Au NPs supported on a well-ordered and clean CeO_2 surface may not be relevant. The surface of industrial-grade oxide supporting material is likely to be highly defected, have broken metal−oxygen bonds, oxygen or metal ion vacancies, grain boundaries, and steps under realistic conditions. Furthermore, the concentration of defects would increase with reduction of the size of the oxide support to the nanoscale. Defects can alter the local stoichiometry of the oxide support and significantly affect the catalytic properties of supported Au NPs. The strong binding between vacancies and Au NPs means that their interactions are inevitable,[18] so the effect of defects on the catalytic properties of the Au NPs must be considered as well.

Received: August 9, 2011
Published: December 19, 2011

dx.doi.org/10.1021/ja207510v | J. Am. Chem.Soc. 2012, 134, 1560−1570

In this work, we used density functional theory (DFT) to study and compare CO oxidation catalyzed by Au_{13} NPs supported on stoichiometric and partially reduced CeO_2 surfaces. We optimized the structure of gas-phase Au_{13} NPs and subsequently supported them on CeO_2 surfaces. We find that three different reaction pathways, two of them are dependent upon the nature of the supporting oxide, contribute to the overall rate of CO oxidation. On the basis of the reaction mechanisms, we suggest a strategy for the design of CeO_2-supported Au catalyst for CO oxidation.

METHODS

Choice of Au Nanoparticle: Size and Structure. Current computational resources are insufficient to study supported Au NP catalysis on experimental time and length scales. Hence, choosing the most appropriate size and shape of Au NPs is critical for studies involving model systems. In a recent report, Zhang et al. investigated fcc or hcp-like crystalline two-layer closed-packed CeO_2-supported Au NPs.[19] These clusters were generated by depositing Au atoms onto the CeO_2 surface with a single oxygen vacancy,[19] a process that is relevant to physical deposition in high-vacuum conditions. Their conclusion was that a hcp-like Au_{11} NP was likely to be present on the surface and to be catalytically active. In this work, we considered Au_9 and Au_{10} clusters of structure similar to the Au_{11} cluster, except with the topmost capping Au atom removed[19] to avoid this atom's unrealistically low coordination number (see Figure 1 of ref 19). We examined the stability of these structures on CeO_2 with a single vacancy (CeO_2-1VAC) and three triangular surface vacancies (CeO_2-3VAC). We also tested the stability of these clusters with adsorbed CO and O_2 molecules (see Figure S1).

We found that, as Zhang et al. reported,[19] fcc-like Au_9 and hcp-like Au_{10} NPs were stable on CeO_2-1VAC. However, the Au−Au atomic bonds of Au_{10}@CeO_2-3VAC, which has a hexagonal bottom layer structure, are unfavorably stretched (Figure S1(c,d)). Au_9, which has a triangular bottom layer configuration, remained stable on CeO_2-3VAC but deformed upon O_2 and CO adsorption (Figure S1(b,e,f)). Although fcc or hcp-like small Au NPs were found to be the most stable structures on CeO_2-1VAC, they became unstable when the number of vacancies in CeO_2 increased. Likely, the strong interaction between Au atoms and oxygen vacancies induces structural deformation of Au_9 and Au_{10} NPs.

To find other Au NP structures, which could be more stable when supported on CeO_2 at oxygen vacancies under CO oxidation conditions, we modeled particles that are known to be stable when formed with capping-ligands in solution. This chemical synthesis process is the most promising method for the mass production of NPs.[23] Two sizes of ligand-covered small Au NPs can be found in the literature.[24−26] Häkkinen and co-workers did calculations of a ligand-covered Au_{11} NP of the size that was studied by Zhang et al. and reported the CO oxidation mechanism.[26] The Frenkel and Nuzzo groups reported that monodispersed ligand-capped icosahedral (Ih) Au_{13} NPs are stable in solution.[25] They also successfully supported ligand-capped Au_{13}-Ih NPs on anatase-TiO_2.[24] It is this Au_{13} cluster that we used to generate a stable supported Au nanoparticle. To do this, we initially optimized unsupported Au_{13} NPs in vacuum conditions and then reoptimized the most stable isomers on a CeO_2 support. The Au_{13} cluster was found to be stable upon CO or O_2 adsorption, so we used the Au_{13}@CeO_2-STO and Au_{13}@CeO_2-3VAC in our CO oxidation studies. To test the sensitivity of our results with respect to particle size and structure, the most important steps for CO oxidation were repeated on the Au_9 and Au_{10} clusters and were shown to be consistent with that acquired from Au_{13}.

Computational Details. Initial structures of Au_{13} NPs were generated from molecular dynamic simulations at 300 K using the quantum Sutton−Chen many-body potential.[27] More than 10 three-dimensional initial structures, as well as previously reported planar and cage structures,[28] were optimized at the GGA-level with spin-polarized DFT. For structure optimization, we used an all-electron scalar relativistic basis set[29] as implemented in the DMol^3 code.[30] The exchange-correlation energy was evaluated with the PBE functional,[31] and the orbital cutoff range was 5.0 Å. We used a Fermi smearing method with a width of 0.007 hartree. The energy, force, and displacement convergence criteria were set to 10^{-5} hartree, 0.002 hartree/Å, and 0.005 Å, respectively.

The CeO_2 support was described with a 4 × 4 CeO_2(111) slab with 6 atomic layers and 20 Å of vacuum (Figure 1). The three upper layers

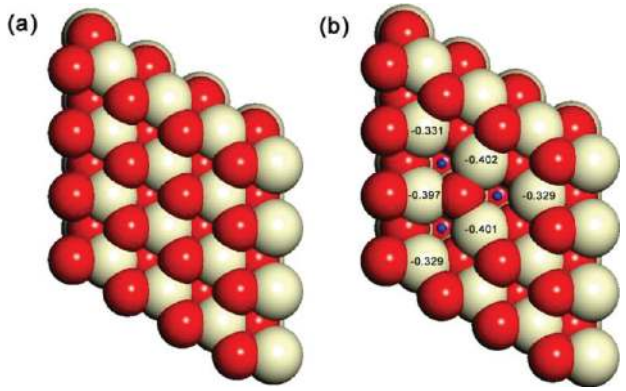

Figure 1. A 4 × 4 CeO_2(111) slab was used to model (a) stoichiometric CeO_2 and (b) partially reduced CeO_2 with three vacancies. A change in Bader charge due to the presence of the vacancies (shown in adjacent Ce ions) confirms that Ce ions are partially reduced from Ce^{4+} to Ce^{3+}. Blue small spheres show the vacancy sites; ivory and red spheres represent Ce and O atoms.

of the CeO_2 slab were relaxed during geometry optimization. Experiments on vacancy formation in the CeO_2 surface showed that a linear oxygen trivacancy is preferred to a triangular vacancy,[16] whereas DFT calculations predict a triangular structure as the most stable (in our calculation, a triangular trivacancy is more stable by as much as 0.16 eV). Esch et al. reported that diffusion of single oxygen vacancies in the CeO_2 surface and their polymerization requires thermal energy.[16] The morphology and distribution of single and poly oxygen vacancies in the CeO_2 surface and their effect on electron localization are highly complicated.[32−34] In this study, we are focusing on the effect of the presence of oxygen vacancy and reduced Ce^{3+} ions on CO oxidation by CeO_2-supported Au NPs. Thus, we chose the DFT-predicted triangular trivacancy to maximize the interaction between the vacancies, the partially reduced Ce^{3+} ions, and the supported Au_{13} NP. While the morphology and the concentration of oxygen vacancies could affect CO oxidation by Au on CeO_2, this consideration is outside the scope of our current work.

We performed spin-polarized DFT calculations in a plane-wave basis with the VASP code[35] using the PBE[31] functional. To treat highly localized Ce 4f-orbital, DFT+U[36] with U_{eff} = 5 was applied. The plane wave energy cutoff was 400 eV, and ionic cores were described by the PAW method implemented in VASP.[37] The Brillouin zone was sampled at the Γ-point. The convergence criteria for the electronic structure and the geometry were 10^{-4} eV and 0.01 eV/Å, respectively. We used the Gaussian smearing method with a finite temperature width of 0.1 eV to improve convergence of states near the Fermi level. The location and energy of transition states (TSs) were calculated with the climbing-image nudged elastic band method.[38]

RESULTS AND DISCUSSION

Structural Optimization of Au_{13}@CeO_2-STO and Au_{13}@CeO_2-3VAC. Strong relativistic effects in Au lead to its unique electronic structure, which includes a contracted 6s shell and a significant s−d hybridization.[39−41] The relativistic effects stabilize a planar structure in small Au clusters.[28,39] The relativistic effect is prominent even in larger Au NPs consisting of more than 60 atoms.[42] Nørskov and co-workers have

dx.doi.org/10.1021/ja207510v | J. Am. Chem.Soc. 2012, 134, 1560−1570

reported that the structure of TiO_2-supported Au NPs is quite flexible during CO oxidation.[6] Structural evolution of Au NPs is observed in various size ranges.[42−44]

When the structure of a Au NP evolves upon adsorption, it is difficult to separate the intrinsic affinity of the adsorbate to the Au NP from the additional contribution caused by the structural change. We therefore minimize the structural evolution of Au NPs during the reaction by using highly stable Au_{13} NP on CeO_2.

To find a sufficiently stable structure of supported Au_{13}, we optimized Au_{13} NPs in the gas phase and then again on the CeO_2 surface. Figure 2 shows the planar geometry of Au_{13} that

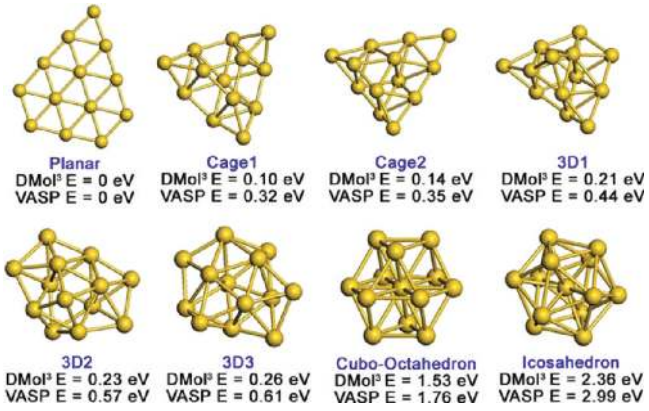

Figure 2. Eight stable structures of the Au_{13} NP. Cohesive energies are relative to the most stable planar structure calculated with two different DFT codes. All-electron-based DMol³ calculations generally predict a narrower energy gap between isomers as compared to the pseudopotential-based VASP calculations.

is the most stable structure in the gas phase. Regardless of the structure, all Au_{13} isomers took a doublet spin state (S = 1/2). Because the energy differences between isomers were found to be small, we supported each isomer on both the stoichiometric CeO_2-STO and partially reduced CeO_2-3VAC surfaces.

Ce^{4+} ions in CeO_2 have an empty 4f-orbital that will partially fill as Ce^{4+} ions are reduced to Ce^{3+} (see Figure 1b).[45] Figure 3

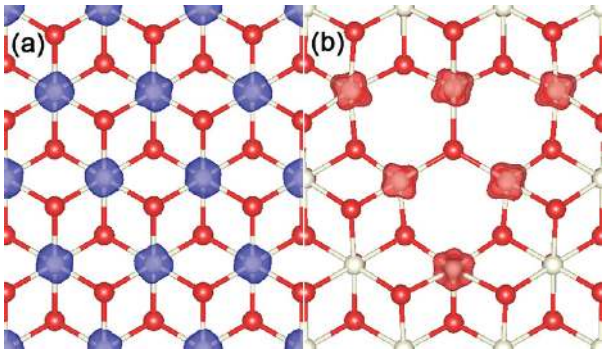

Figure 3. The geometry of the frontier orbital in CeO_2 surface is shown: (a) an empty 4f orbital is the LUMO and localized to Ce^{4+} ions of CeO_2-STO, and (b) a partially filled 4f orbital is the HOMO and localized to Ce^{3+} ions of CeO_2-3VAC.

shows the LUMO of CeO_2-STO and HOMO of CeO_2-3VAC. The LUMO of CeO_2-STO is a 4f-orbital localized on the Ce^{4+} ions, and the three oxygen vacancies reduce the six nearest Ce^{4+} ions to Ce^{3+} with a ferromagnetic spin ordering, such that s = 6/2. The energy difference between the ferromagnetic and antiferromagnetic, s = 0, spin states is less than 0.05 eV, which is in agreement with a previous report.[34]

Ganduglia-Pirovano et al.[34] and Li et al.[33] independently found that reducing the nearest neighbor Ce^{4+} ions of a single oxygen vacancy is not energetically favorable. The vacancy prefers to be bound to Ce^{4+} ions; therefore, two Ce^{3+} ions would be created away from the oxygen vacancy.[34] In our triangularly ordered trivacancy model, the six neighboring Ce^{4+} ions were reduced to Ce^{3+}. The difference is that the previous studies evaluated the effect of only a single oxygen vacancy. Possible reasons for the observed stability of the well-ordered distribution of Ce^{3+} ions in our calculations include a lack of subsurface oxygen vacancies and polymerization of single oxygen vacancies.

Consistent with experimental observations,[18] Au_{13} preferentially binds to the oxygen vacancy, and the binding energy of Au_{13} increases with the number of the oxygen vacancies (Table S1). Planar Au_{13} is found to be unstable when supported on CeO_2-STO and CeO_2-3VAC (see Figure 4); a three-dimensional structure was favored in both cases.

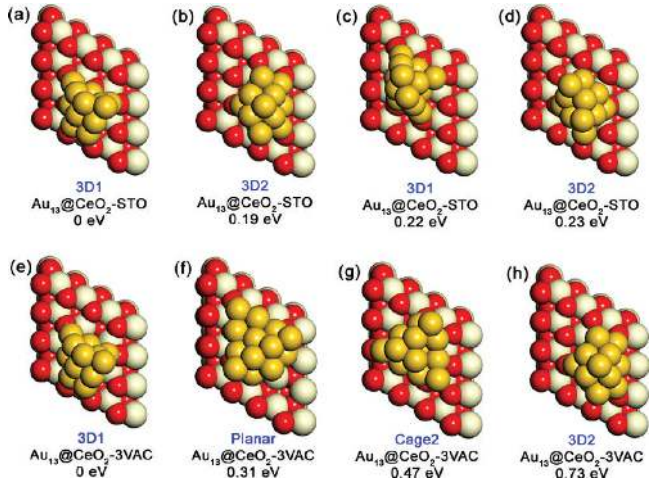

Figure 4. The four most stable geometries of Au_{13} supported on CeO_2-STO (a−d) and CeO_2-3VAC (e−h). The blue name indicates the original structure of the gas-phase Au_{13} NP (shown in Figure 2). Energy values are with respect to the most stable structure.

To compare CO oxidation by Au_{13} supported on CeO_2-STO and CeO_2-3VAC, we used a single structure of the Au_{13} cluster that was sufficiently stable on both supports. As presented in Figure 4, the (a,e) and (b,h) pairs satisfy this requirement. Even though the (a,e) pair (hereafter, A) is the most stable structure energetically, we instead decided to use the second-most stable structure, the (b,h) pair (hereafter, B), for the following reason.

The exceptional stability of the structures in A (also refer to *xyz* coordinates in the Supporting Information) is likely due to the Au(111) microfacet composed of 8 atoms on the side of Au_{13}. This is natural because they were generated from the cage 1 structure shown in Figure 2, which has a banded Au(111) microfacet. As a result, Au atoms that do not belong to the microfacet have more distorted and loosely packed structure when supported, and therefore the average coordination number (CN) of the second and third layer Au atoms of A is low, 5.43. This is lower than the average CN of B, 5.71. Moreover, Figure 4 also shows that the lowest-coordinated top

dx.doi.org/10.1021/ja207510v | J. Am. Chem.Soc. 2012, 134, 1560−1570

Au atom of A has only three neighboring Au atoms. Such low atomic coordination is an unrealistic model for larger Au NPs; it is rather a special case of small NPs. In the case of B, there is no asymmetric distortion, which can influence the O oxidation calculation. We have therefore selected the B model for further catalysis studies even though the B was less stable than the A. We found that the B model structure remained stable during CO oxidation.

Electronic Interaction between CeO_2 and Au NP. A Bader charge[46,47] and frontier orbital analysis of the electron interaction between Au_{13} and CeO_2-STO and CeO_2-3VAC shows that the empty 4f-orbital localized on Ce^{4+} ions of CeO_2-STO, the LUMO of CeO_2-STO, draws electrons from supported Au_{13}. Similarly, Au_{13} attracts electrons from the HOMO of CeO_2-3VAC, the 4f-orbital of Ce^{3+} ions (Figures 3, 5, and 6). One of

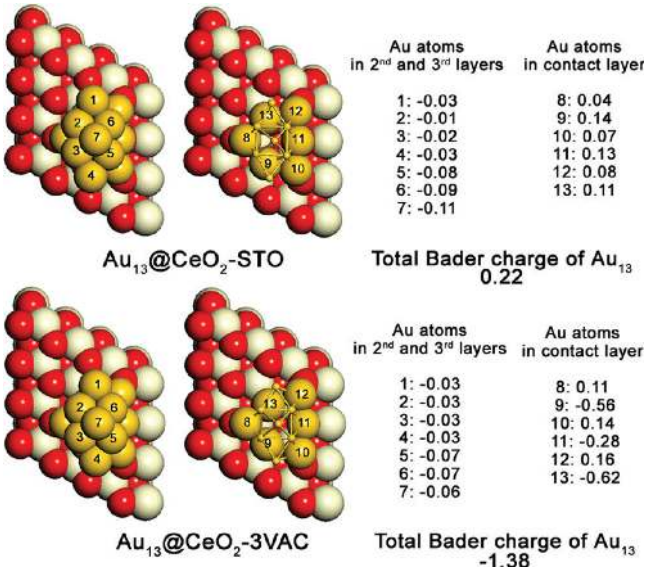

Figure 5. The HOMO of a CeO_2-supported Au_{13} NP is shown. The HOMO of Au_{13}@CeO_2-STO is plotted in (a)−(c). The HOMO of Au_{13}@CeO_2-3VAC is plotted in (d)−(f). To show electrons localized in the 4f orbital of Ce atoms, the Au_{13} NP was cut in (c) and (f). An empty 4f orbital of CeO_2-STO draws electrons from supported Au_{13} NP and becomes the HOMO, whereas the Au_{13} NP attracts electrons from some of the partially filled Ce^{3+} ions of CeO_2-3VAC.

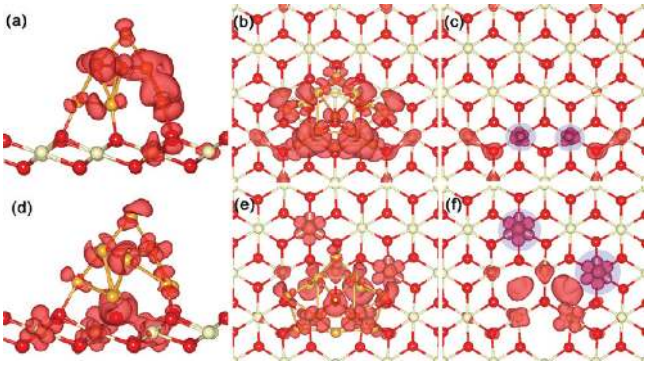

Figure 6. Bader charge analysis on Au_{13}@CeO_2-STO and Au_{13}@CeO_2-3VAC is shown. Electronic interaction between Au_{13} NP and CeO_2 is localized to contacting layer Au atoms.

the Ce^{3+} ions in Au_{13}@CeO_2-3VAC is, thus, the second nearest neighbor from the oxygen vacancy, as predicted by Li et al.[33] and Ganduglia-Pirovano et al.[34] (see Figure 5f). Electron transfer between Au_{13} and CeO_2-STO positively charges Au_{13}, whereas electron transfer between Au_{13} and CeO_2-3VAC negatively charges Au_{13}. We find that the relative stability of isolated Au_{13} isomers is sensitive to their charge state (Table S2), so the destabilization of a planar Au_{13} on the CeO_2 surface could be related to electron transfer. Charge transfer would change the valence electron configuration of Au and affect the strength of highly directional s−d hybridization. We postulate that a broken balance of s−d hybridization due to electron transfer from or to the Au_{13} supplies a driving force for structural evolution. Our results show that the structure of oxide-supported small Au NPs would be quite different from the stable structure of isolated Au NPs. This distinction is important, because small crystalline Au NPs, such as Au_{12}[2] and Au_{13} cuboctahedron,[21] have been used so far as a representative of supported small Au NPs for computational studies.

Bader charge analysis[46,47] shows that, although the total charge state of Au_{13} on CeO_2-STO and CeO_2-3VAC is quite different (Figure 5), the electronic interaction is localized in the layer of Au atoms that are in direct contact the substrate. Au atoms in noncontacting layers, the second and third layers in the Au cluster, are less affected by the electronic interaction. The energy of adsorption of CO and O_2 is highly sensitive to the electronic state of the adsorption site.[21,48−50] We find, however, that CO and O_2 prefer to bind to the under-coordinated Au atoms in noncontacting layers as opposed to negatively or positively charged Au ions.

CO Oxidation by Coadsorbed CO and O_2 on Au_{13} of Au_{13}@CeO_2. CO and O_2 adsorption were tested on Au_{13}@CeO_2-STO and Au_{13}@CeO_2-3VAC (see Figure S2 for details). The most favorable CO−O_2 coadsorption geometry with the highest coadsorption energy was selected for further CO oxidation studies. Complete CO oxidation by coadsorbed CO and O_2 on Au in Au_{13}@CeO_2-STO is shown in Figure 7a. The energies of adsorption show that Au_{13} strongly binds CO (−1.05 eV) but binds O_2 relatively weakly (−0.56 eV). Coadsorbed CO and O_2 can react to form a gas-phase CO_2 and a residual Au−O* on Au_{13} in a −1.64 eV exothermic process with a 0.14 eV activation barrier. We found that the residual Au−O* can directly react with an additional gas-phase CO molecule. Another possible CO oxidation pathway following the formation of Au−O* is the association of Au−O* and Au−CO* to produce CO_2, as shown in Figure S3a. Both CO oxidation pathways from the Au−O* intermediate proceed spontaneously, so the life-span of the Au−O* should be very short.

Figure 7b shows that the presence of oxygen vacancies on the surface of CeO_2 does not affect the mechanism of CO oxidation. Oxygen vacancies strengthen O_2 binding to Au_{13}@CeO_2-3VAC from −0.56 to −0.76 eV. The formation of a gas-phase CO_2 from coadsorbed Au−CO* and Au−O_2*, with a 0.33 eV activation barrier, is the rate-determining step of the reaction.

A microkinetic analysis on the CO oxidation by CeO_2-supported Au_{13} NPs shows that CO binds more strongly to Au_{13}@CeO_2-STO than does O_2 leading to a low O_2 coverage (see Table 1). The stronger O_2 binding to Au_{13}@CeO_2-3VAC leads to a 10 times higher adsorbed O_2 concentration. However, Table 1 shows that the higher energy barrier for CO oxidation in Au_{13}@CeO_2-3VAC, due to the increased stability of the adsorbed state (stage 1 in Figure 7b), lowers the CO oxidation rate.

dx.doi.org/10.1021/ja207510v | J. Am. Chem.Soc. 2012, 134, 1560−1570

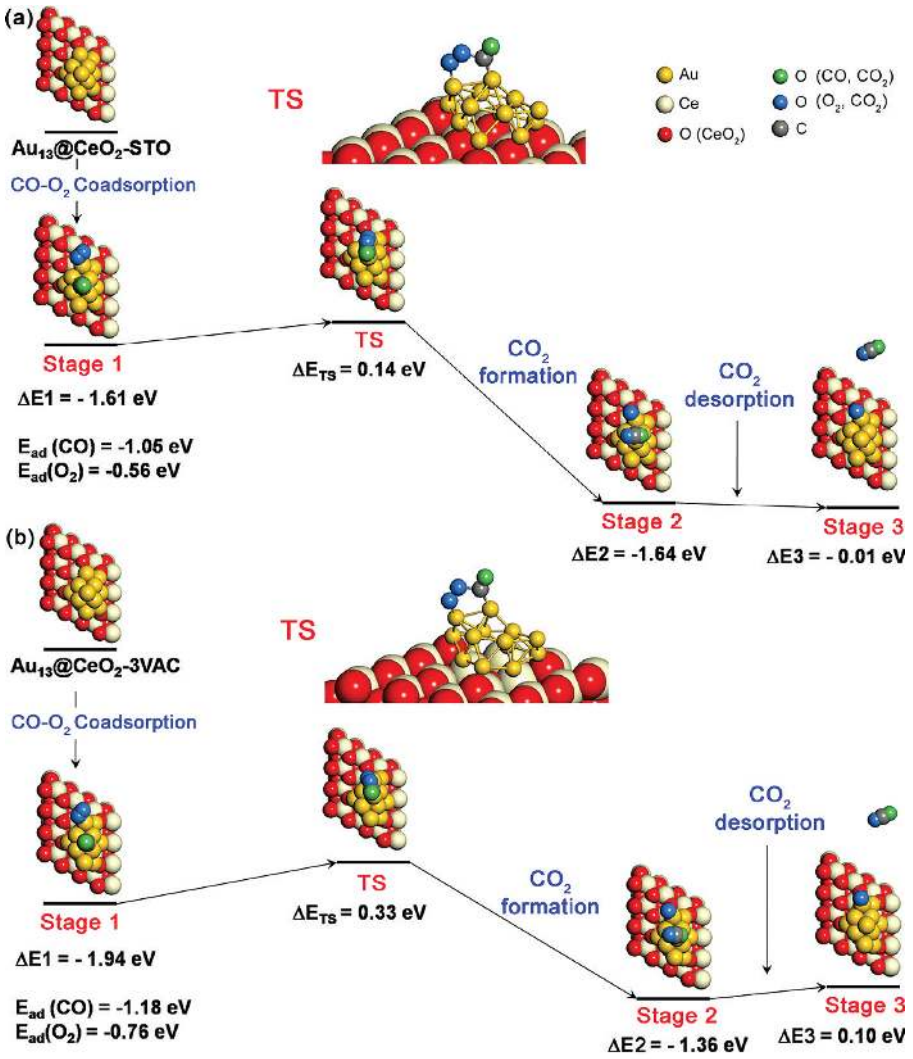

Figure 7. CO oxidation by Au_{13} of CeO_2-supported Au_{13} NPs is shown with $Au_{13}@CeO_2$-STO in (a) and $Au_{13}@CeO_2$-3VAC in (b). ΔEx is the energy of the xth stage relative to that of the previous stage; for example, $\Delta E3$ is the energy difference between stage 3 and stage 2. ΔE_{TS} is the energy of the TS relative to the previous state.

Table 1. Microkinetic Analysis on CO Oxidation by CO and O_2 Coadsorbed on $Au_{13}@CeO_2$-STO and $Au_{13}@CeO_2$-3VAC[a]

	energy of CO adsorption (eV)	energy of O_2 adsorption (eV)	barrier (eV)	rate(R3)^{max} (S^{-1})	θ_{O_2}
$Au_{13}@CeO_2$-STO	−1.05	−0.56	0.14	7.01×10^3	2.63×10^{-7}
$Au_{13}@CeO_2$-3VAC	−1.18	−0.76	0.33	6.55×10^1	4.02×10^{-6}

[a]The maximum reaction rate on $Au_{13}@CeO_2$-3VAC can be acquired by increasing the energy of O_2 adsorption from −0.76 to −1.08 eV (4.07×10^6 S^{-1}, θ_{O_2} = 0.51) with fixed CO adsorption energy (−1.18 eV) or decreasing the energy of CO adsorption from −1.18 to −0.86 eV (4.02×10^6 S^{-1}, θ_{O_2} = 0.51). The maximum rate was acquired when the ratio of the energy of O_2 and CO adsorption is approximately 0.9.

Experimental and theoretical studies on CO oxidation by oxide-supported Au NPs report a wide range of barriers for CO oxidation, depending on the cluster size and the supporting oxide.[51−56] Our calculated barrier for CO oxidation by $Au_{13}@CeO_2$ is at the lower limit of reported values. Campbell and co-workers reported an experimental barrier of 0.12 ± 0.02 eV for CO oxidation by two-layer Au islands on TiO_2, which is comparable to our case of $Au_{13}@CeO_2$-STO.[52] Theoretical studies on CO oxidation by TiO_2- or MgO-supported small Au NPs reported a barrier between 0.1 and 0.5 eV.[55,56]

The balance of the CO and O_2 adsorption energies, as well as the reaction barrier, accounts for the CO oxidation rate by coadsorbed CO and O_2. Increasing the energy of O_2 adsorption on $Au_{13}@CeO_2$-3VAC from −0.76 to −1.08 eV leads to the 1000 times higher CO oxidation rate (4.07×10^6 S^{-1}). The maximum reaction rate of CO oxidation was acquired when the ratio of the energy of O_2 adsorption and CO adsorption (O_2/CO) is 0.90. Because strong adsorption leads to increased energy barriers, lowering the energy of CO adsorption rather than increasing the O_2 adsorption energy is more effective for increasing the CO oxidation rate. Strong CO adsorption on Pt NPs blocks active sites or destabilizes other adsorbates, leading to CO poisoning.[57] We found that this is the case for small Au NPs as well. As presented by Nilekar et al. in transition metal-Pt shell NPs,[57] modifying Au NPs with alloying elements would be a promising way for the lower CO adsorption energy and

dx.doi.org/10.1021/ja207510v | J. Am. Chem.Soc. 2012, 134, 1560−1570

the lower and higher saturated CO and O_2 concentration, respectively.

The presence of oxygen vacancies and Ce^{3+} ions in the CeO_2 surface does not significantly influence the intrinsic CO oxidation activity of CeO_2-supported Au_{13}. CO oxidation at under-coordinated Au atoms confirms that this process is independent from effects due to the metal−oxide interface and charged Au ions.

Freund and co-workers showed that a corner atom of MgO-supported Au NP reduces its charge state from −0.21 e to +0.16 e upon CO adsorption due to Pauli repulsion with the CO-5σ orbital,[48] which is consistent with our findings. We found that the Au atom binding CO was positively charged upon CO adsorption (+0.17 e and +0.15 e in Au_{13}@CeO_2-STO and Au_{13}@CeO_2-3VAC, respectively). A Bader charge analysis,[46,47] presented in Figure S4, shows that electrons from the Au atom binding CO were redistributed over all of the Au atoms in Au_{13}@CeO_2-3VAC, whereas on Au_{13}@CeO_2-STO the electrons (0.29 e) were largely transferred to the empty 4f-band of Ce atoms, leading to more positively charged Au_{13} (see Figure S4a). The same amount of charge was transferred to the adsorbed O_2 molecule in both Au_{13}@CeO_2-STO and Au_{13}@CeO_2-3VAC, mostly from the nearest Au atom. Because both CeO_2 supports equally activate the O_2 molecule, and because the O_2 adsorption is quite localized, we postulate that the increased energy of O_2 adsorption on Au_{13}@CeO_2-3VAC does not originate from the excess electrons in Au atoms of Au_{13}@CeO_2-3VAC. Rather, destabilization of electrophilic Au NP due to charge loss to Ce atoms upon CO−O_2 coadsorption is presumably responsible for the lower coadsorption energy of Au_{13}@CeO_2-STO. Note that the Au NP in Au_{13}@CeO_2-STO lost 0.77 e to O_2 and CeO_2, whereas the Au NP in Au_{13}@CeO_2-3VAC donated 0.37 e, mostly to O_2. Table S3 shows that Au_{13}-3D2 used in this study becomes highly unstable when the NP is positively charged.

Evaluating the reactive regions of Au NPs and their charge state has been a central issue for rational catalyst design. Both positively charged[13,58] and negatively charged Au ions[59,60] have been suggested as a reactive center. Other studies instead suggest oxygen vacancies,[61,62] a metal−oxide interface,[63,64] or metallic corner atoms[65] as reactive species. The complete CO oxidation pathway and rate presented in Figure 7 and Table 1 show that charged Au ions play no direct role in CO oxidation, because CO and O_2 preferentially bind to noncontacting Au atoms with low-coordination numbers.

The rate of CO oxidation by coadsorbed CO and O_2 at under-coordinated Au atoms would depend on the surface fraction of the under-coordinated Au atoms. Even though Au_{13}

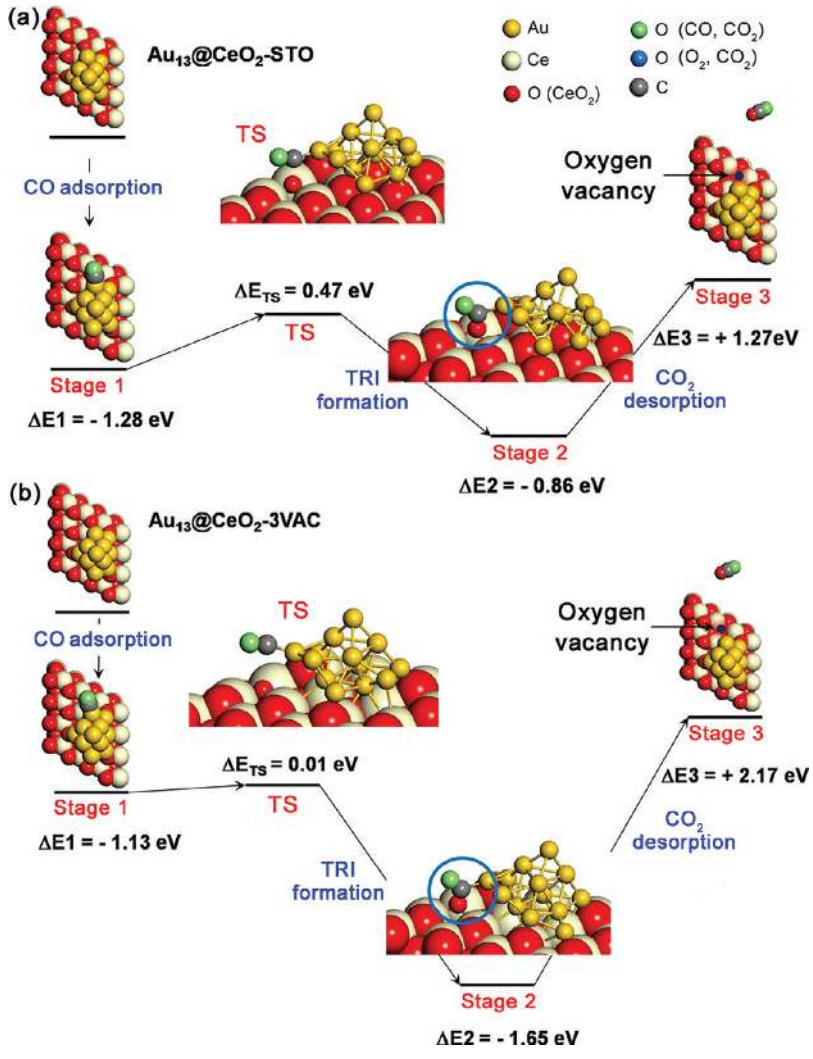

Figure 8. The first half of CO oxidation by M-vK mechanism, oxidation of CO on Au_{13} by a lattice oxygen atom of CeO_2 support, is shown. Au_{13}@CeO_2-STO is plotted in (a) and Au_{13}@CeO_2-3VAC in (b).

dx.doi.org/10.1021/ja207510v | J. Am. Chem.Soc. 2012, 134, 1560−1570

catalyzes CO oxidation by itself, the contribution of this direct CO oxidation by Au NP may decrease as the size of Au NP increases. The role of linear corner atoms rather than individual under-coordinated Au atoms would become important in larger Au NPs, as was recently shown by Shang and Liu.[66]

An increase in the O_2 adsorption energy due to the presence of oxygen vacancies in the surface was also seen for the Au_9@CeO_2-3VAC model (details are described in Figure S1).

CO Oxidation by Lattice Oxygen of CeO_2 and CO on Au_{13}: Mars–van Krevelen Mechanism. Camellone and Fabris reported that a lattice oxygen of CeO_2 oxidizes CO when bound to a Au adatom.[13] CO oxidation by the Mars–van Krevelen (M-vK) mechanism, in which the oxide directly binds CO, is commonly observed in several modified oxide catalysts, as well.[20,67] We examined CO oxidation at the Au–CeO_2 interface and found that, contrary to the typical M-vK mechanism, the Au NP binds CO during oxidation.

Figure 8 shows the first half of the CO oxidation process by the M-vK mechanism. Au_{13} strongly binds a CO molecule by −1.28 eV in Au_{13}@CeO_2-STO and −1.13 eV in Au_{13}@CeO_2-3VAC. We find that Au–CO* and an adjacent lattice oxygen atom in the CeO_2 support associate to form a triangular reaction intermediate (TRI). Formation of a TRI is highly exothermic with a 0.47 eV energy barrier in Au_{13}@CeO_2-STO and a 0.01 eV energy barrier in Au_{13}@CeO_2-3VAC. Subsequent CO_2 desorption, however, requires 1.27 eV for Au_{13}@CeO_2-STO and 2.17 eV for Au_{13}@CeO_2-3VAC.

This pathway is equivalent to removing a single oxygen atom from CeO_2 and oxidizing a gas-phase CO molecule to CO_2. We find that, because of the high stability of TRI, it is difficult to compensate for the vacancy formation energy with the CO_2 formation energy, and, thus, this leads to a high CO_2 desorption energy. In a low temperature regime, it is probable that the TRI acts as a spectator rather than a reaction intermediate. Entropic contribution to the Gibbs free energy of CO_2 desorption (TS) is −0.66 eV at 298 K (standard entropy of CO_2 is 213.79 J mol^{-1} K^{-1} at 1 atm).[68] Therefore, spontaneous CO_2 desorption would be a rare event at room temperature (or below) and prevent direct participation of lattice oxygen of CeO_2 in CO oxidation. Camellone and Fabris,

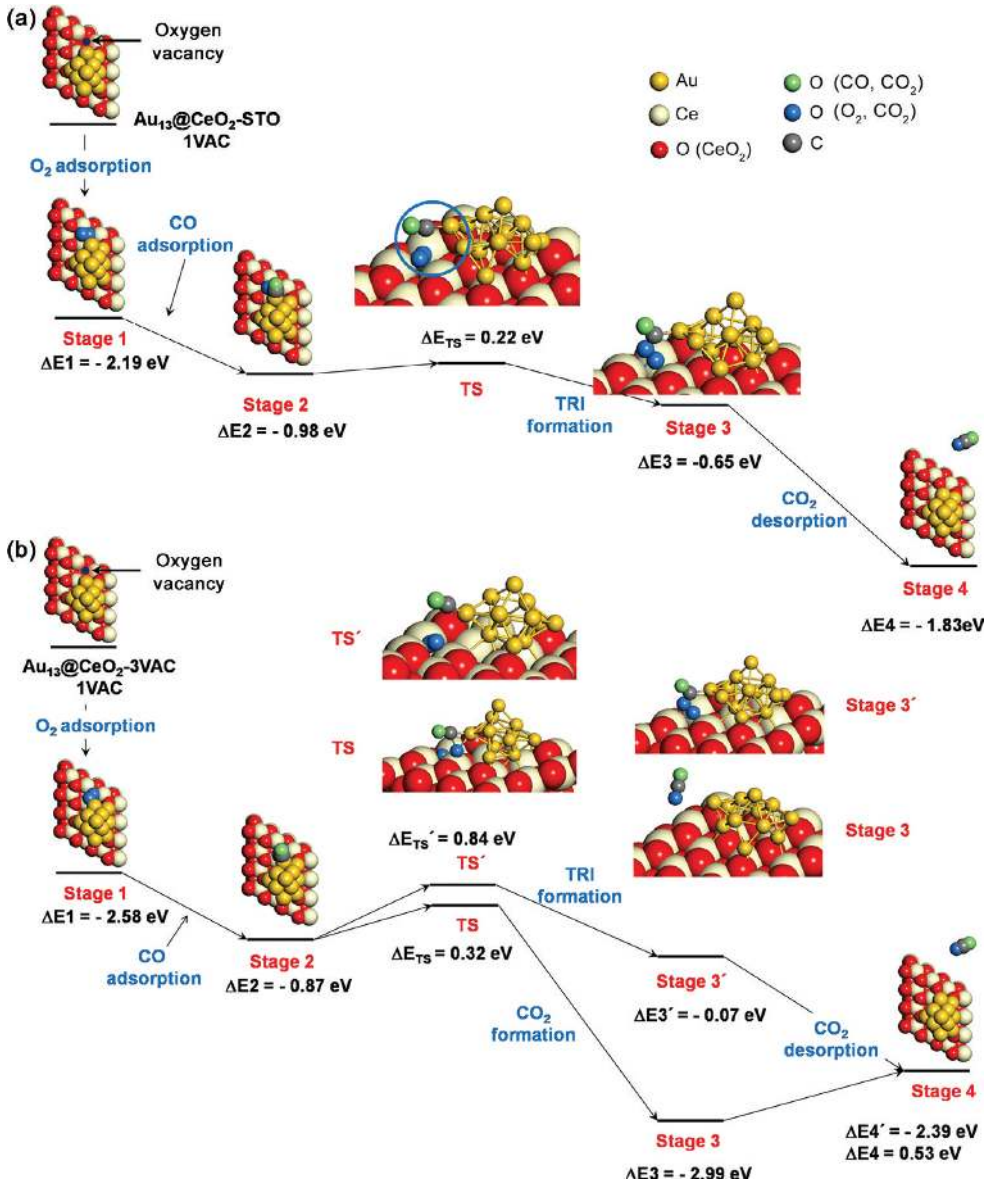

Figure 9. The second half of CO oxidation by the M-vK mechanism is shown for (a) Au_{13}@CeO_2-STO and (b) Au_{13}@CeO_2-3VAC.

dx.doi.org/10.1021/ja207510v | J. Am. Chem.Soc. 2012, 134, 1560–1570

in contrast, considered a single, mobile Au adatom, which could bind with an oxygen vacancy and stabilize the system.[13]

Metiu and co-workers have suggested that dopants can lower the vacancy formation energy of the host oxide and, thus, promote the oxidation reaction by the M-vK mechanism.[20,67,69,70] The vacancy formation energy of Au-doped CeO_2 is negative, which means an oxygen vacancy can form spontaneously in the presence of a Au dopant.[20,69] The rate-determining step in the reaction, CO_2 desorption from TRI (see Figure 8), is directly related to the vacancy formation in the CeO_2 surface. The enthalpy of CO oxidation is a constant −3.26 eV, so the energy of vacancy formation is the only factor that determines the total reaction energy. From a catalysis design perspective, this relationship indicates that lowering the vacancy formation energy of CeO_2 will lower the CO_2 desorption energy from TRI. Using a doped CeO_2 as a supporting oxide for Au NPs would activate CO oxidation by opening this additional low-temperature reaction pathway.

Figure 9 shows the second half of the CO oxidation process. As a part of the M-vK mechanism of CO oxidation, a surface oxygen vacancy on CeO_2 strongly binds a gas-phase O_2 molecule ($V-O_2$*) and results in vacancy healing (see stage 1 of Figure 9a and b). The energy of O_2 adsorption is stronger by 0.39 eV in the reduced surface due to the difference in vacancy formation energy on CeO_2-STO and CeO_2-3VAC. This trend is consistent with O_2 adsorption on modified oxides reported by Metiu and co-workers; the oxygen vacancy of easily reducible oxides weakly binds an O_2 molecule.[67]

In the case of Au_{13}@CeO_2-STO, Au−CO* and $V-O_2$* associate into the TRI with an enthalpy of −0.65 eV and a 0.22 eV energy barrier. CO_2 dissociation from TRI is exothermic by −1.83 eV, so CO_2 is produced spontaneously, and the surface oxygen vacancy is healed. On the other hand, a formation energy of −0.07 eV and a correspondingly high energy barrier of 0.84 eV show that the formation of TRI is a rare event in Au_{13}@CeO_2-3VAC. Rather, Au−CO* and a protruding O atom of $V-O_2$* can be directly associated to a gas-phase CO_2 with a lowered energy barrier, 0.32 eV. In this case, CO_2 formation is highly exothermic by −2.99 eV. An energy of 0.53 eV is needed to completely desorb CO_2 from the surface.

When the oxygen vacancy is healed by gas-phase O_2, the Au_{13}@CeO_2-STO releases the excess surface oxygen to form TRI exothermically with an enthalpy of −0.65 eV. In contrast, Au_{13}@CeO_2-3VAC, which is oxygenphilic, has a low TRI formation energy of −0.07 eV. Direct CO_2 formation from $V-O_2$* and Au−CO* is instead more favorable. The different oxygen affinities of the CeO_2 support significantly alter the available reaction pathways of CO oxidation such that TRI forms in Au_{13}@CeO_2-STO and CO_2 forms directly in Au_{13}@CeO_2-3VAC.

Note that the second cycle of the M-vK mechanism proceeds in the presence of an additional oxygen vacancy, suggesting that the vacancy formation energy affects the CO oxidation reactivity of CeO_2-supported Au NPs. Oxygen vacancies bind gas-phase O_2 molecules and subsequently oxidize Au−CO*.

Au−Ce^{3+} Interface as an Anchoring Site of O_2. Rodriguez et al. recently investigated the role of the Au−CeO_2 interface in the water−gas shift reaction by showing high activity of the inverse catalyst, Au-supported CeO_2 NPs,[71] and suggested a critical role of Ce^{3+} ions.[64,72] The Au−CeO_2 interface does not accelerate CO oxidation by the M-vK mechanism, so we investigated the Au−CeO_2 interface as an additional binding site of reacting molecules. We find that an oxygen molecule would bind to the Au−Ce^{3+} interface due to the excess electron on the Ce^{3+} and note that O_2 adsorption is dependent on the oxidation state of Ce. Other Au−Ce^{4+} bridge sites of Au_{13}@CeO_2-3VAC and Ce^{4+} ions of Au_{13}@CeO_2-STO were not able to bind an O_2 molecule as strongly. Therefore, we conclude that the oxygen vacancy, where the Au NP anchors, reduces adjacent Ce^{4+} to Ce^{3+} and provides an additional CO oxidation pathway in which CO reacts with O_2 at a Au−Ce^{3+} interface.

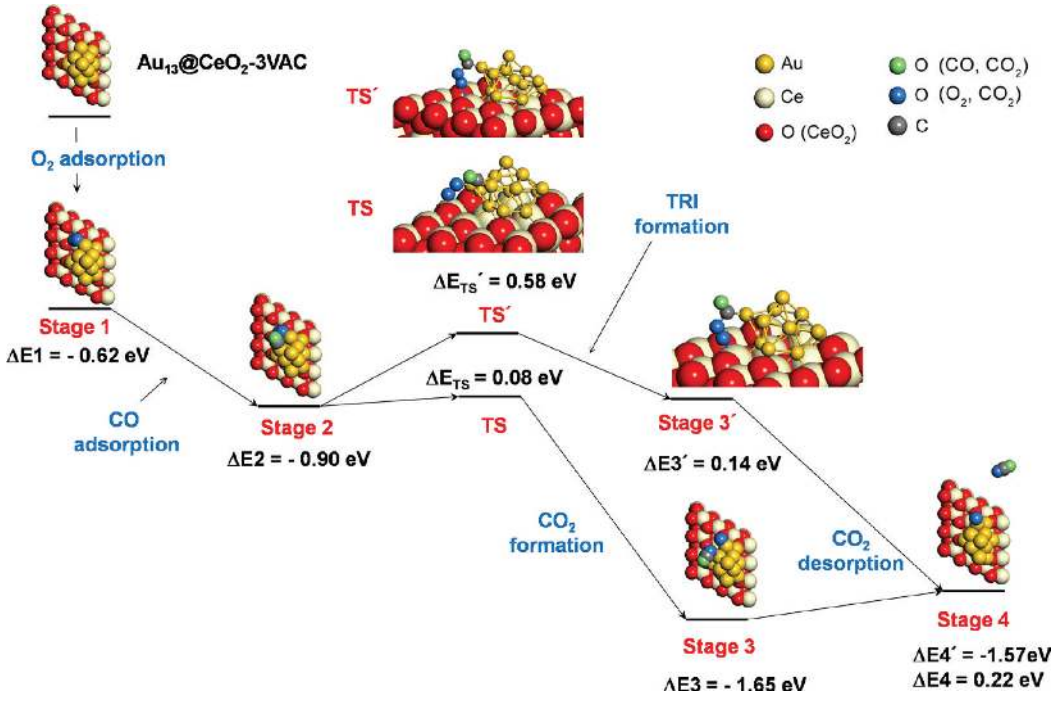

Figure 10. CO oxidation by O_2 adsorbed to Au−Ce^{3+} bridge site is shown. Direct CO_2 production is preferred to CO oxidation through TRI formation.

dx.doi.org/10.1021/ja207510v | J. Am. Chem.Soc. 2012, 134, 1560−1570

Figure 10 shows the complete CO oxidation mechanism with O_2 adsorbed on the Au−Ce^{3+} interface and CO on Au_{13}. CO on Au_{13} and O_2 at an Au−Ce^{3+} interface directly dissociated into CO_2 and Au−O*. Direct CO_2 dissociation is highly exothermic by −1.65 eV with a low energy barrier of 0.08 eV. Another possible pathway can proceed through TRI formation from Au−CO* and O_2 at a Au−Ce^{3+}; this pathway is slightly endothermic by 0.14 eV, and the dissociation to CO_2 and Au−O* is highly exothermic by −1.57 eV. An energy barrier of 0.58 eV is required for TRI formation, so CO oxidation through TRI formation would be less favorable than direct CO_2 dissociation. The rest of the reaction proceeds as described in Figure S3(b). Because only 0.22 eV is needed to activate CO oxidation by the Au−Ce^{3+} interface, this process is operational at low temperature. There is a physical bond between the product CO_2 and the Au NP (see stage 3 of Figure 10). Considering the entropic contribution to CO_2 desorption (discussed earlier), we postulate that this process is spontaneous and does not lower the CO_2 production rate. The enthalpy of this step is almost equal to the energy required to activate CO oxidation by under-coordinated Au atoms; however, this pathway's contribution will become more critical as the size of Au NPs increases and thus widens the Au−CeO_2 interface.

Because the Au−Ce^{3+} interface binds an O_2 molecule, CO would readily adsorb on Au_{13} without competition for the same adsorption site. This process operates only in the presence of reduced Ce^{3+} ions, which are a direct consequence of pre-existing oxygen vacancies. The role of the interface between supported Au NPs and the CeO_2 support is to supply an additional reaction pathway by O_2 adsorbed to Au−Ce^{3+} bridge site and separate O_2 and CO adsorption sites. Oxygen vacancies that reduce adjacent Ce^{4+} of CeO_2 to Ce^{3+} ions are essential in activating CO oxidation by the Au−Ce^{3+} interface.

Recently, Green et al. reported the CO oxidation mechanism by the O_2 bound to the Au−Ti bridging site, which is consistent with our finding.[73]

Nanosize Effect of the CeO_2 Support. We used the CeO_2(111) surface throughout this study; however, as the dimension of CeO_2 support decreases from surface to nanoparticle, the concentration of the Ce^{3+} ions increases due to dangling bonds. It has been shown that the Ce^{3+}/Ce^{4+} ratio is higher in small CeO_2 clusters[74,75] and Ce^{3+} ions preferentially occupy under-coordinated sites, edge or corner sites.[76] High concentration of Ce^{3+} ions in stepped CeO_2 surface was also reported.[77]

Vayssilov et al. recently showed that oxygen transfer from the CeO_2 support to Pt NPs, termed oxygen spillover, occurs due to the low vacancy formation energy of nanostructured CeO_2.[78] The oxygen spillover was not observed in our case because of high vacancy formation energy of the CeO_2 surface; it has never been reported with Au NPs. Their findings, however, confirm that the size of CeO_2 support has a critical role in catalytic activity of supported NPs.

Carrettin et al. showed that the activity of CO oxidation catalyzed by Au on CeO_{2-x} NPs of ∼4 nm diameter is 2 orders of magnitude larger than that of Au on bulk CeO_2.[79] A low vacancy formation energy of CeO_{2-x} NPs[78,80] would accelerate CO oxidation by the M-vK mechanism combined with adsorbed O_2 at the Au−Ce^{3+} anchoring site.

CONCLUSION

Herein, we investigate the origin of CO oxidation activity of CeO_2-supported Au NPs by investigating various CO oxidation pathways. On the basis of DFT+U calculations, we suggest the following CO oxidation pathways by CeO_2-supported Au NPs: CO oxidation by coadsorbed CO and O_2 at Au_{13} NPs, CO oxidation by lattice oxygen of CeO_2 and Au−CO*, and CO oxidation by O_2 adsorbed to the Au−Ce^{3+} interface.

The underlying properties of the Au NPs, such as under-coordinated Au atoms, create a CO oxidation pathway by coadsorbed CO and O_2. Pre-existing oxygen vacancies in the CeO_2 surface did not alter the reaction pathway for catalysis on the Au NP. Contrary to previous studies, we found that positively or negatively charged Au ions have no direct effect on the pathway and rate of CO oxidation. Oxygen vacancies in the CeO_2 surface strengthen O_2 binding to Au NP and increase the O_2 surface concentration. The high energy barrier, however, due to a stabilized reactant state compensates for the influence of the increased O_2 adsorption energy on CO oxidation activity.

The second process, the M-vK mechanism of CO oxidation by the Au−CeO_2 interface, requires a higher energy and is only active at high temperature. If the vacancy concentration in the CeO_2 surface is high, however, pre-existing vacancies can bind the O_2 molecule and oxidize a Au−CO* by the second half of the M-vK mechanism.

Oxygen vacancies in CeO_2 create Ce^{3+} ions and open a new CO oxidation pathway by O_2 adsorbed on Au−Ce^{3+} bridge site. The contribution of this third process would be higher in easily reducible oxides.

Our findings on the mechanism of CO oxidation catalyzed by Au NPs supported on stoichiometric and partially reduced CeO_2 confirm a critical role of oxygen vacancy in the CeO_2 surface on CO oxidation activity of CeO_2-supported Au NP, providing a theoretical guideline on the design of highly reactive catalysis in the supported NP class.

We suggest that lowering the vacancy formation energy of the supporting oxide using easily reducible oxides or modifying the oxides is promising for higher CO oxidation reactivity by three possible mechanisms: (1) activating the M-vK mechanism of CO oxidation by lowering the energy of CO_2 production, (2) increasing the number of oxygen vacancies in the CeO_2 surface that bind and supply O_2 for the second half of the M-vK mechanism, and (3) increasing the concentration of reduced metal ions, which act as anchoring sites for O_2 molecules.

ASSOCIATED CONTENT

Supporting Information

Details on microkinetic analysis and additional data presented in tables (S1−S3) and figures (S1−S4). This material is available free of charge via the Internet at http://pubs.acs.org.

AUTHOR INFORMATION

Corresponding Author

hykim8083@gmail.com

ACKNOWLEDGMENTS

This work is supported by the Department of Energy under contract DE-SC0001091. All calculations were done at the National Energy Research Scientific Computing Center. H.Y.K. thanks Zachary D. Pozun for careful reading of this manuscript. H.M.L. is grateful for financial support from the Future-based Technology Development Program (Nano Fields) through the National Research Foundation of Korea (NRF) funded by the Ministry of Education, Science, and Technology (2011-0019163).

REFERENCES

(1) Haruta, M.; Kobayashi, T.; Sano, H.; Yamada, N. *Chem. Lett.* **1987**, *16*, 405.
(2) Falsig, H.; Hvolbaek, B.; Kristensen, I. S.; Jiang, T.; Bligaard, T.; Christensen, C. H.; Norskov, J. K. *Angew. Chem., Int. Ed.* **2008**, *47*, 4835.
(3) Hakkinen, H.; Abbet, W.; Sanchez, A.; Heiz, U.; Landman, U. *Angew. Chem., Int. Ed.* **2003**, *42*, 1297.
(4) Roldan, A.; Gonzalez, S.; Ricart, J. M.; Illas, F. *ChemPhysChem* **2009**, *10*, 348.
(5) Yoon, B.; Koskinen, P.; Huber, B.; Kostko, O.; von Issendorff, B.; Hakkinen, H.; Moseler, M.; Landman, U. *ChemPhysChem* **2007**, *8*, 157.
(6) Lopez, N.; Norskov, J. K. *J. Am. Chem. Soc.* **2002**, *124*, 11262.
(7) Remediakis, I. N.; Lopez, N.; Norskov, J. K. *Angew. Chem., Int. Ed.* **2005**, *44*, 1824.
(8) Yoon, B.; Hakkinen, H.; Landman, U.; Worz, A. S.; Antonietti, J. M.; Abbet, S.; Judai, K.; Heiz, U. *Science* **2005**, *307*, 403.
(9) Liu, Z. P.; Gong, X. Q.; Kohanoff, J.; Sanchez, C.; Hu, P. *Phys. Rev. Lett.* **2003**, *91*, 266102.
(10) Molina, L. M.; Hammer, B. *J. Chem. Phys.* **2005**, *123*, 161104.
(11) Molina, L. M.; Rasmussen, M. D.; Hammer, B. *J. Chem. Phys.* **2004**, *120*, 7673.
(12) Rodriguez, J. A.; Evans, J.; Graciani, J.; Park, J. B.; Liu, P.; Hrbek, J.; Sanz, J. F. *J. Phys. Chem. C* **2009**, *113*, 7364.
(13) Camellone, M. F.; Fabris, S. *J. Am. Chem. Soc.* **2009**, *131*, 10473.
(14) Liu, Z. P.; Jenkins, S. J.; King, D. A. *Phys. Rev. Lett.* **2005**, *94*, 196102.
(15) Zhang, C. J.; Michaelides, A.; Jenkins, S. J. *Phys. Chem. Chem. Phys.* **2010**, *13*, 22.
(16) Esch, F.; Fabris, S.; Zhou, L.; Montini, T.; Africh, C.; Fornasiero, P.; Comelli, G.; Rosei, R. *Science* **2005**, *309*, 752.
(17) Lawrence, N. J.; Brewer, J. R.; Wang, L.; Wu, T. S.; Wells-Kingsbury, J.; Ihrig, M. M.; Wang, G. H.; Soo, Y. L.; Mei, W. N.; Cheung, C. L. *Nano Lett.* **2011**, *11*, 2666.
(18) Baron, M.; Bondarchuk, O.; Stacchiola, D.; Shaikhutdinov, S.; Freund, H. J. *J. Phys. Chem. C* **2009**, *113*, 6042.
(19) Zhang, C. J.; Michaelides, A.; King, D. A.; Jenkins, S. J. *J. Am. Chem. Soc.* **2010**, *132*, 2175.
(20) Shapovalov, V.; Metiu, H. *J. Catal.* **2007**, *245*, 205.
(21) Roldan, A.; Ricart, J. M.; Illas, F.; Pacchioni, G. *Phys. Chem. Chem. Phys.* **2010**, *12*, 10723.
(22) Wang, H. F.; Gong, X. Q.; Guo, Y. L.; Guo, Y.; Lu, G. Z.; Hu, P. *J. Phys. Chem. C* **2009**, *113*, 6124.
(23) Park, J.; An, K. J.; Hwang, Y. S.; Park, J. G.; Noh, H. J.; Kim, J. Y.; Park, J. H.; Hwang, N. M.; Hyeon, T. *Nat. Mater.* **2004**, *3*, 891.
(24) Xu, H.; Menard, L.; Frenkel, A.; Nuzzo, R.; Johnson, D.; Yang, J. *The Effect of Substrates/Ligands on Metal Nanocatalysts Investigated By Quantitative Z Contrast Imaging and High Resolution Electron Microscopy*; Materials Research Society Symposium Proceedings, 2005; Materials Research Society: San Francisco, 2005; p R9.4/P6.4.
(25) Guliamov, O.; Frenkel, A. I.; Menard, L. D.; Nuzzo, R. G.; Kronik, L. *J. Am. Chem. Soc.* **2007**, *129*, 10978.
(26) Lopez-Acevedo, O.; Kacprzak, K. A.; Akola, J.; Hakkinen, H. *Nat. Chem.* **2010**, *2*, 329.
(27) Cagin, T.; Che, J. W.; Gardos, M. N.; Fijany, A.; Goddard, W. A. *Nanotechnology* **1999**, *10*, 278.
(28) Shafai, G.; Hong, S. Y.; Bertino, M.; Rahman, T. S. *J. Phys. Chem. C* **2009**, *113*, 12072.
(29) Koelling, D. D.; Harmon, B. N. *J. Phys. C: Solid State Phys.* **1977**, *10*, 3107.
(30) Delley, B. *J. Chem. Phys.* **2000**, *113*, 7756.
(31) Perdew, J. P.; Burke, K.; Ernzerhof, M. *Phys. Rev. Lett.* **1996**, *77*, 3865.
(32) Torbrugge, S.; Reichling, M.; Ishiyama, A.; Morita, S.; Custance, O. *Phys. Rev. Lett.* **2007**, *99*, 056101.
(33) Li, H. Y.; Wang, H. F.; Gong, X. Q.; Guo, Y. L.; Guo, Y.; Lu, G. Z.; Hu, P. *Phys. Rev. B* **2009**, *79*, 193401.
(34) Ganduglia-Pirovano, M. V.; Da Silva, J. L. F.; Sauer, J. *Phys. Rev. Lett.* **2009**, *102*, 026101.
(35) Kresse, G.; Furthmuller, J. *Phys. Rev. B* **1996**, *54*, 11169.
(36) Dudarev, S. L.; Botton, G. A.; Savrasov, S. Y.; Humphreys, C. J.; Sutton, A. P. *Phys. Rev. B* **1998**, *57*, 1505.
(37) Blochl, P. E. *Phys. Rev. B* **1994**, *50*, 17953.
(38) Henkelman, G.; Uberuaga, B. P.; Jonsson, H. *J. Chem. Phys.* **2000**, *113*, 9901.
(39) Hakkinen, H.; Moseler, M.; Landman, U. *Phys. Rev. Lett.* **2002**, *89*, 033401.
(40) Pyykko, P. *Chem. Rev.* **1988**, *88*, 563.
(41) Pyykko, P. *Angew. Chem., Int. Ed.* **2004**, *43*, 4412.
(42) Huang, W.; Ji, M.; Dong, C. D.; Gu, X.; Wang, L. M.; Gong, X. G.; Wang, L. S. *ACS Nano* **2008**, *2*, 897.
(43) Shao, N.; Huang, W.; Gao, Y.; Wang, L. M.; Li, X.; Wang, L. S.; Zeng, X. C. *J. Am. Chem. Soc.* **2010**, *132*, 6596.
(44) Hakkinen, H.; Moseler, M.; Kostko, O.; Morgner, N.; Hoffmann, M. A.; von Issendorff, B. *Phys. Rev. Lett.* **2004**, *93*, 093401.
(45) Ganduglia-Pirovano, M. V.; Hofmann, A.; Sauer, J. *Surf. Sci. Rep.* **2007**, *62*, 219.
(46) Henkelman, G.; Arnaldsson, A.; Jonsson, H. *Comput. Mater. Sci.* **2006**, *36*, 354.
(47) Tang, W.; Sanville, E.; Henkelman, G. *J. Phys.: Condens. Matter* **2009**, *21*, 084204.
(48) Lin, X.; Yang, B.; Benia, H. M.; Myrach, P.; Yulikov, M.; Aumer, A.; Brown, M. A.; Sterrer, M.; Bondarchuk, O.; Kieseritzky, E.; Rocker, J.; Risse, T.; Gao, H. J.; Nilius, N.; Freund, H. J. *J. Am. Chem. Soc.* **2010**, *132*, 7745.
(49) Kim, H. Y.; Han, S. S.; Ryu, J. H.; Lee, H. M. *J. Phys. Chem. C* **2010**, *114*, 3156.
(50) Roldan, A.; Ricart, J. M.; Illas, F.; Pacchioni, G. *J. Phys. Chem. C* **2010**, *114*, 16973.
(51) Aguilar-Guerrero, V.; Gates, B. C. *J. Catal.* **2008**, *260*, 351.
(52) Bondzie, V. A.; Parker, S. C.; Campbell, C. T. *Catal. Lett.* **1999**, *63*, 143.
(53) Zhou, Z.; Flytzani-Stephanopoulos, M.; Saltsburg, H. *J. Catal.* **2011**, *280*, 255.
(54) Huang, X. S.; Sun, H.; Wang, L. C.; Liu, Y. M.; Fan, K. N.; Cao, Y. *Appl. Catal., B* **2009**, *90*, 224.
(55) Sanchez, A.; Abbet, S.; Heiz, U.; Schneider, W. D.; Hakkinen, H.; Barnett, R. N.; Landman, U. *J. Phys. Chem. A* **1999**, *103*, 9573.
(56) Remediakis, I. N.; Lopez, N.; Norskov, J. K. *Appl. Catal., A* **2005**, *291*, 13.
(57) Nilekar, A. U.; Alayoglu, S.; Eichhorn, B.; Mavrikakis, M. *J. Am. Chem. Soc.* **2010**, *132*, 7418.
(58) Fu, Q.; Saltsburg, H.; Flytzani-Stephanopoulos, M. *Science* **2003**, *301*, 935.
(59) Hagen, J.; Socaciu, L. D.; Elijazyfer, M.; Heiz, U.; Bernhardt, T. M.; Woste, L. *Phys. Chem. Chem. Phys.* **2002**, *4*, 1707.
(60) Hakkinen, H.; Landman, U. *J. Am. Chem. Soc.* **2001**, *123*, 9704.
(61) Wang, X.; Rodriguez, J. A.; Hanson, J. C.; Perez, M.; Evans, J. *J. Chem. Phys.* **2005**, *123*, 221101.
(62) Rodriguez, J. A.; Perez, M.; Evans, J.; Liu, G.; Hrbek, J. *J. Chem. Phys.* **2005**, *122*, 241101.
(63) Park, J. B.; Graciani, J.; Evans, J.; Stacchiola, D.; Ma, S. G.; Liu, P.; Nambu, A.; Sanz, J. F.; Hrbek, J.; Rodriguez, J. A. *Proc. Natl. Acad. Sci. U.S.A.* **2009**, *106*, 4975.
(64) Park, J. B.; Graciani, J.; Evans, J.; Stacchiola, D.; Senanayake, S. D.; Barrio, L.; Liu, P.; Sanz, J. F.; Hrbek, J.; Rodriguez, J. A. *J. Am. Chem. Soc.* **2010**, *132*, 356.
(65) Williams, W. D.; Shekhar, M.; Lee, W. S.; Kispersky, V.; Delgass, W. N.; Ribeiro, F. H.; Kim, S. M.; Stach, E. A.; Miller, J. T.; Allard, L. F. *J. Am. Chem. Soc.* **2010**, *132*, 14018.
(66) Shang, C.; Liu, Z.-P. *J. Am. Chem. Soc.* **2011**, *133*, 9938.
(67) Kim, H. Y.; Lee, H. M.; Pala, R. G. S.; Shapovalov, V.; Metiu, H. *J. Phys. Chem. C* **2008**, *112*, 12398.
(68) Atkins, P.; Paula, J. D. *Physical Chemistry*, 8th ed.; Oxford: New York, 2006.
(69) Nolan, M.; Verdugo, V. S.; Metiu, H. *Surf. Sci.* **2008**, *602*, 2734.

(70) Chretien, S.; Metiu, H. *Catal. Lett.* **2006**, *107*, 143.
(71) Rodriguez, J. A.; Ma, S.; Liu, P.; Hrbek, J.; Evans, J.; Perez, M. *Science* **2007**, *318*, 1757.
(72) Rodriguez, J. A.; Graciani, J.; Evans, J.; Park, J. B.; Yang, F.; Stacchiola, D.; Senanayake, S. D.; Ma, S. G.; Perez, M.; Liu, P.; Sanz, J. F.; Hrbek, J. *Angew. Chem., Int. Ed.* **2009**, *48*, 8047.
(73) Green, I. X.; Tang, W.; Neurock, M.; J., T. Y. Jr. *Science* **2011**, *333*, 736.
(74) Wu, L. J.; Wiesmann, H. J.; Moodenbaugh, A. R.; Klie, R. F.; Zhu, Y. M.; Welch, D. O.; Suenaga, M. *Phys. Rev. B* **2004**, *69*, 125415.
(75) Tsunekawa, S.; Fukuda, T.; Kasuya, A. *Surf. Sci.* **2000**, *457*, L437.
(76) Neyman, K. M.; Loschen, C.; Bromley, S. T.; Illas, F. *J. Phys. Chem. C* **2007**, *111*, 10142.
(77) Illas, F.; Branda, M. M.; Loschen, C.; Neyman, K. M. *J. Phys. Chem. C* **2008**, *112*, 17643.
(78) Neyman, K. M.; Vayssilov, G. N.; Lykhach, Y.; Migani, A.; Staudt, T.; Petrova, G. P.; Tsud, N.; Skala, T.; Bruix, A.; Illas, F.; Prince, K. C.; Matolin, V.; Libuda, J. *Nat. Mater.* **2011**, *10*, 310.
(79) Carrettin, S.; Concepcion, P.; Corma, A.; Nieto, J. M. L.; Puntes, V. F. *Angew. Chem., Int. Ed.* **2004**, *43*, 2538.
(80) Vayssilov, G. N.; Migani, A.; Neyman, K. *J. Phys. Chem. C* **2011**, *115*, 16081.